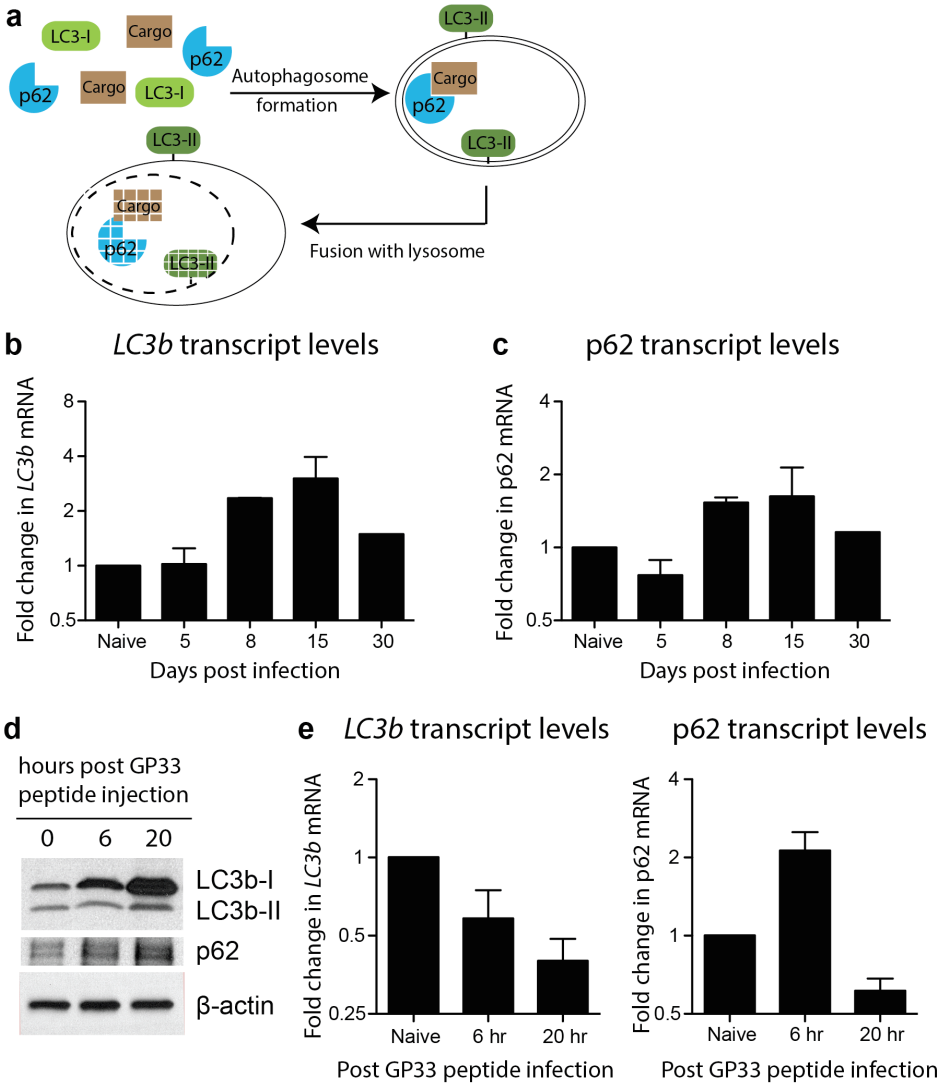

Supplementary Figure 1

Dynamic regulation of autophagy in antigen-specific CD8 T cells.

(**a**) A cartoon illustration of autophagy pathway highlighting molecules that are used to assess autophagy activity in this study. LC3b and p62 are both targeted to autophagosomes, which subsequently fuse with lysosomes for degradation. (**b** and **c**) mRNA levels of *LC3b* (**b**) and p62 (**c**) in P14 at different time points post infection. (**d**) Protein expression levels of LC3b and p62 at early stages of P14 cell activation. GP33 peptide (200 μg) was intraveneously injected into P14 transgenic mice. The corresponding mRNA levels are show in (**e**). Errors bars in (**b**), (**c**) and (**e**) represent SEM. (**b**) - (**e**) are representative of at least two independent experiments.

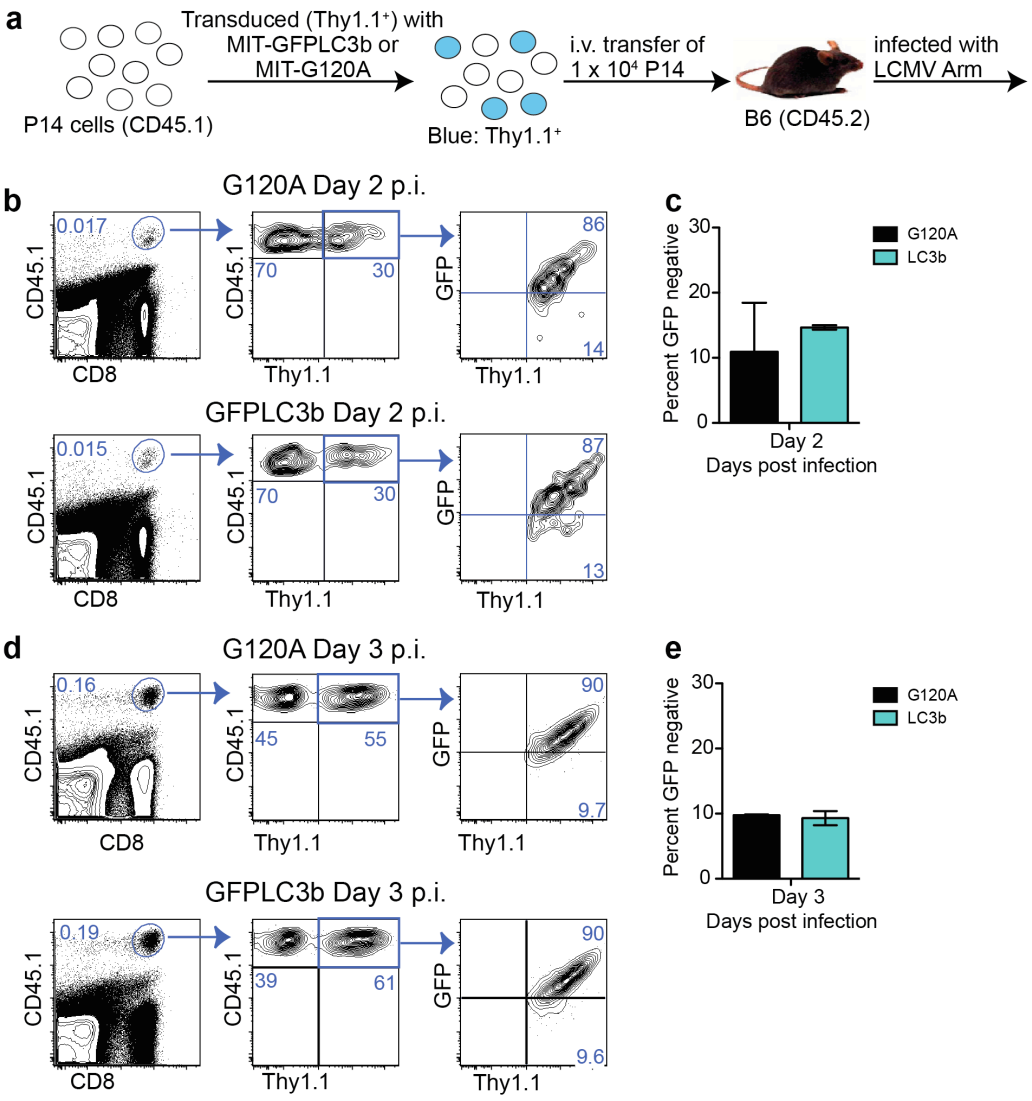

Supplementary Figure 2

Autophagy activity during early expansion phase of CD8 T cells.

(**a**) Experimental set-up. Retrovirus transduced P14 cells were adoptively transferred into B6 mice, followed by LCMV Armstrong infection. (**b-e**) Flow cytometry plots of adoptively transferred P14 cells in spleens. P14 cells transduced with MIT retrovirus harboring GFP-LC3b (either wild type or G120A mutant) are positive for the congenic marker Thy1.1. Day 2 (**b**) and day 3 (**d**) p.i. splenocytes were used for the analysis. The percentage of GFP-negative cells out of the transduced P14 (Thy1.1$^+$) cells from each group is summarized in (**c**) and (**e**). Errors bars in (**c**) and (**e**) represent SEM. (**b**) and (**d**) are representative of two independent experiments, n≥3 in each group.

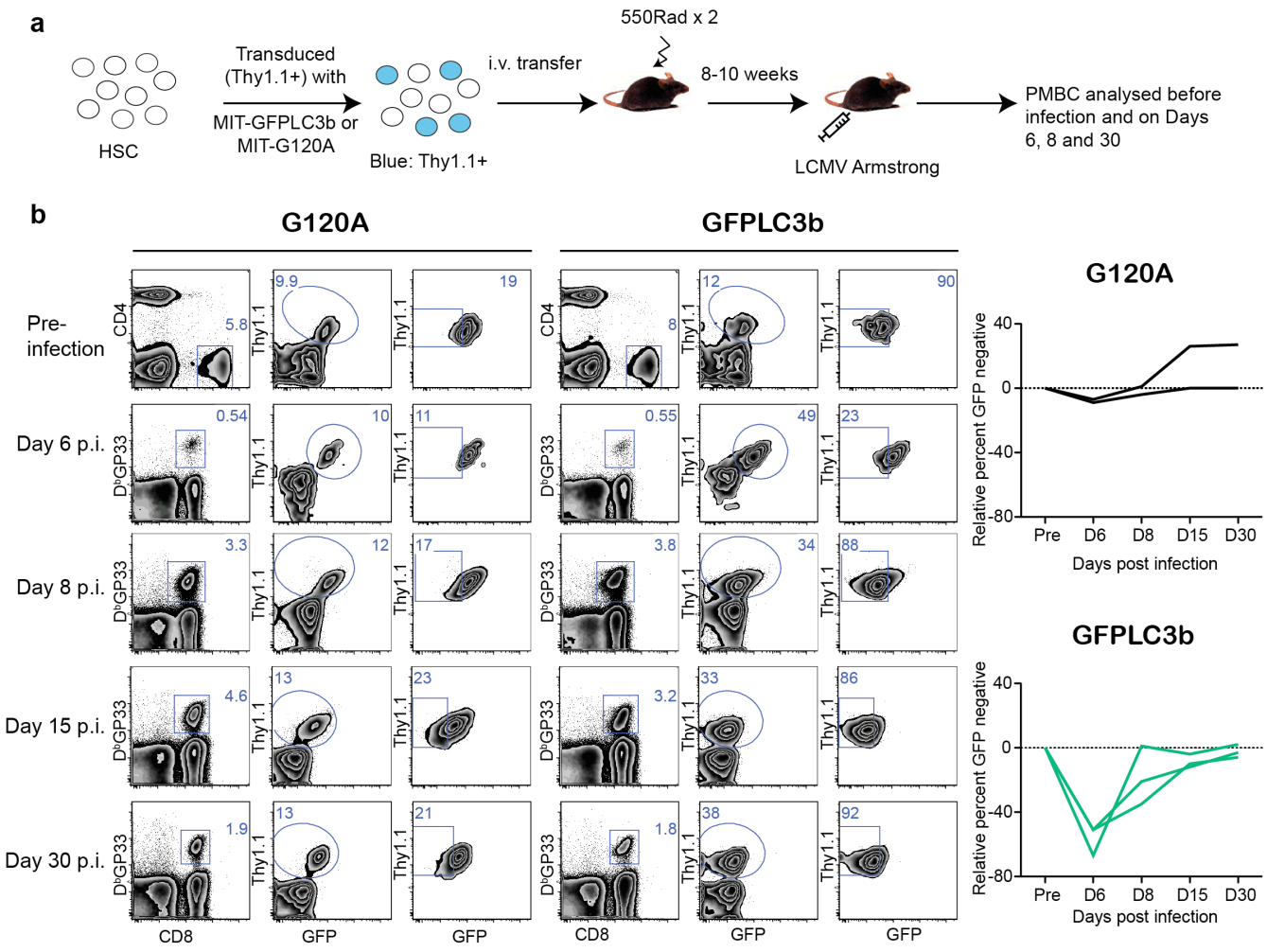

Supplementary Figure 3

Autophagy activity measured in endogenous CD8 T cells using retrovirus carrying reporter gene GFP-LC3b.

(**a**) Experimental set-up. Hematopoietic stem cells transduced with MIT retrovirus harboring GFP-LC3b (either wild type or G120A mutant) were introduced into irradiated host mice, which were left for 8-10 weeks for reconstitution of the hematopoietic system. (b) Flow plots showing changes in GFP intensity over the course of LCMV Armstrong infection in MIT-GFP-LC3b and MIT-G120A groups. Summary plots were shown on the right. (**b**) is representative of two independent experiments, n≥2 in each group.

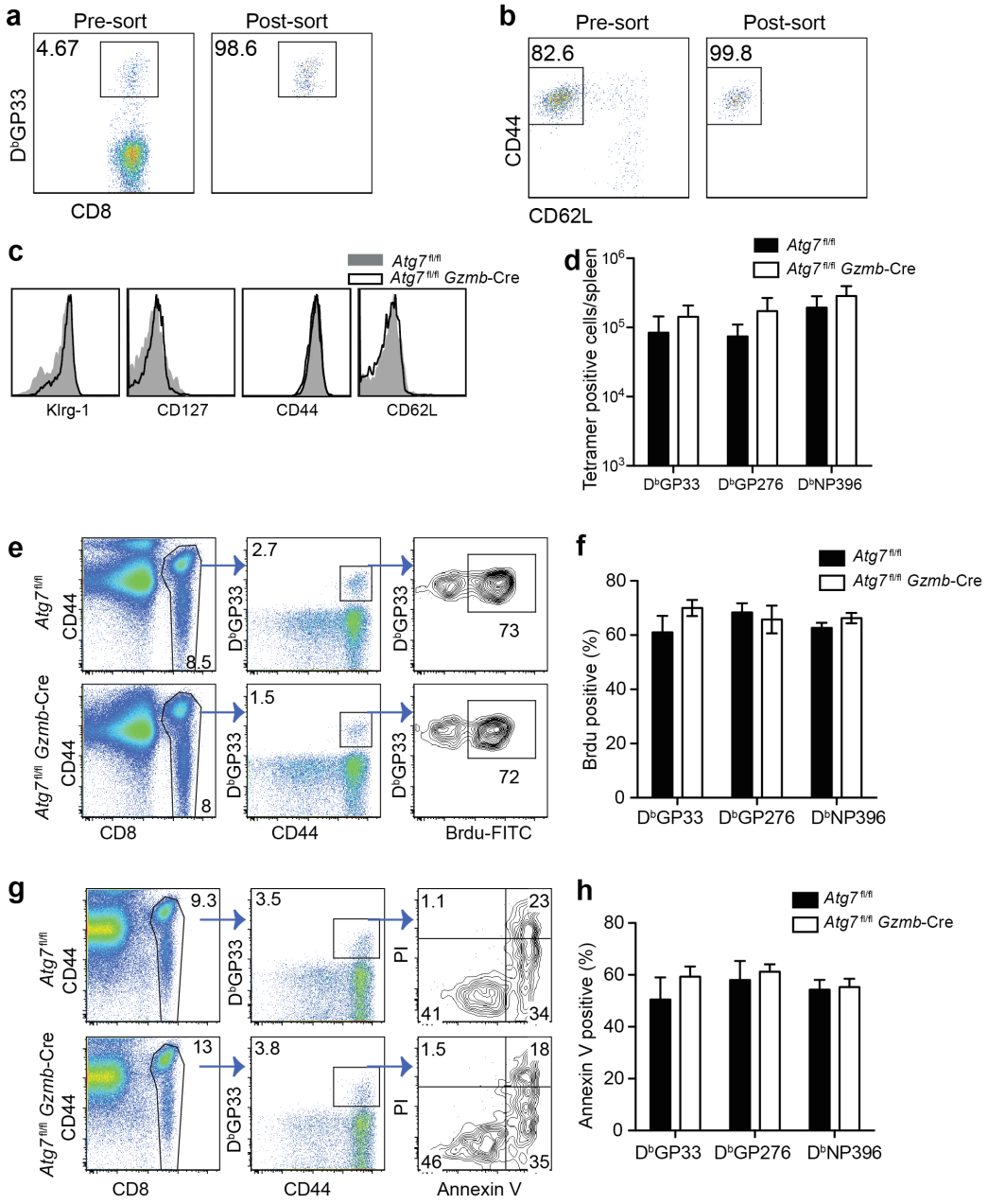

Supplementary Figure 4

Characterization of *Atg7*-deficient DbGP33-specific CD8 T cells.

(**a**) D^bGP33-specific CD8 T cells were purified from day 8 mice infected with LCMV Armstrong ($2x10^5$ pfu). Representative plots of target cells before and after cell sorting, showing a typical > 95% purity. (**b**) Flow cytometry plot of total activated CD8 T cells ($CD44^{hi}CD62L^{lo}$) before and after cell sorting. Spleens were collected from mice infected with LCMV Armstrong ($2x10^5$ pfu) at day 8 p.i.. (**c**) Phenotypic properties of *Atg7*-deficient D^bGP33-specific T cells at day 8 p.i (black outlined histograms). Solid gray histograms represent wild-type D^bGP33-specific T cells. (**d**) Numbers of tetramer-positive cells in spleens 5 days p.i. (**e**) Flow plots showing percent of cells showing Brdu+ 5 hr after Brdu i.p. injection at day 5 p.i.; data summarized in (**f**). (**g**) Flow plots showing percent of cells are Annexin V^+ at day 5 p.i; data summarized in (**h**). Errors bars in (**d**), (**f**) and (**h**) represent SEM. (**c**), (**e**) and (**g**) are representative of at least two independent experiments, n≥3 in each group.

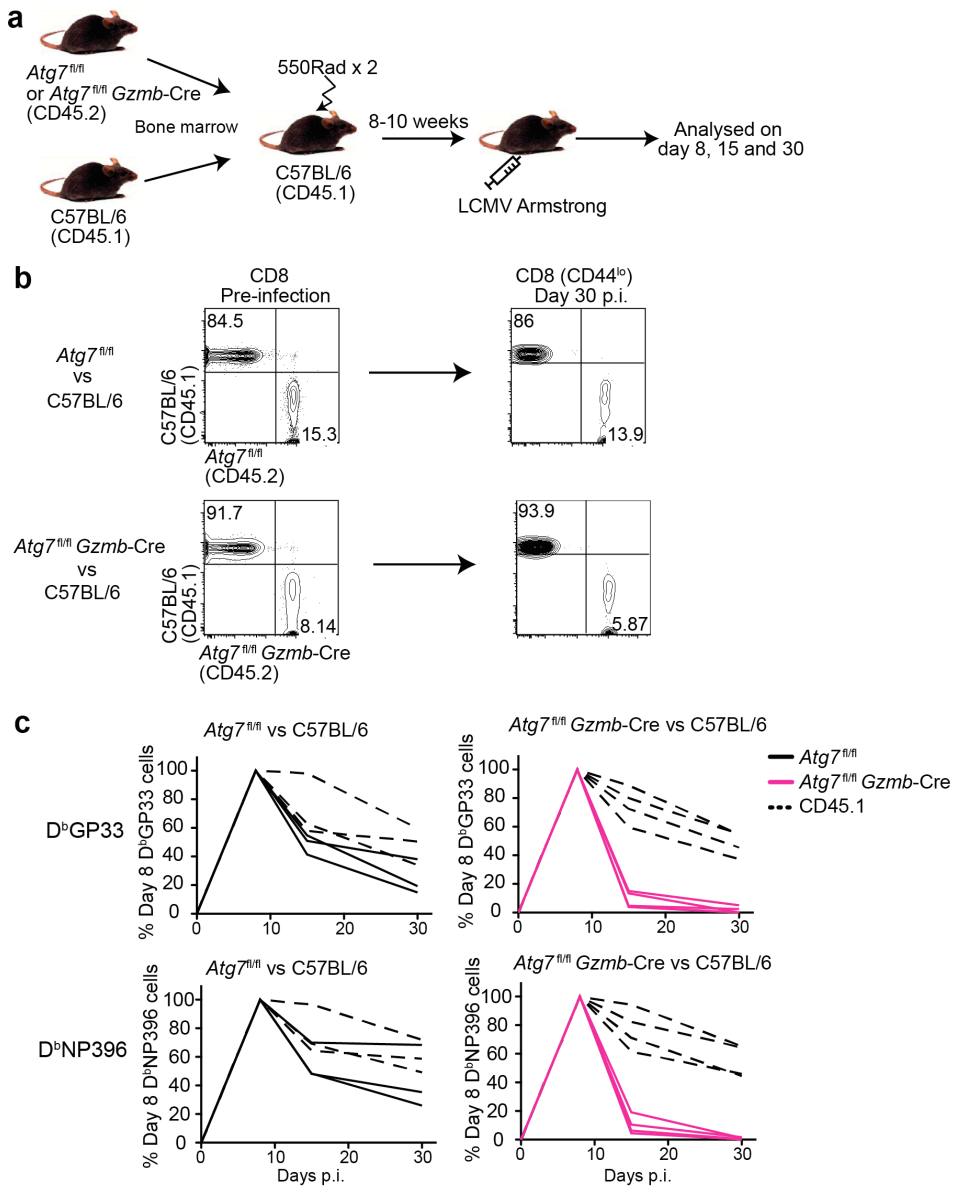

Supplementary Figure 5

Bone marrow chimera reconstitution and T cell response following LCMV Armstrong infection.

(**a**) Experimental set-up for generating *Atg7*$^{fl/fl}$ plus C57BL/6 (CD45.2/CD45.1) control and *Atg7*$^{fl/fl}$ *Gzmb*-Cre plus C57BL/6 (CD45.2/CD45.1) experimental mixed bone marrow chimera mice. CD8 T cell response was evaluated following the LCMV Armstrong infection. (**b**) Peripheral blood mononuclear cells were used to assess the level of reconstitution in the bone marrow chimeras prior to infection. Plots to the right of the arrows indicate the level of reconstitution 30 days p.i in CD44^{lo} populations. Gated on total CD8 T cells. Number on each quadrant represents the percentage of tetramer-positive cells that are either CD45.1^{+} or CD45.2^{+}. (**c**) Summary plot of percentage of D^{b}GP33- and D^{b}NP396-specific T cells from day 8 to day 30 in the peripheral blood of the chimeric mice. The number of tetramer-positive cells on day 8 p.i. is normalized to 100%. The dashed line represents tetramer-positive cell of C57BL/6 origin (CD45.1^{+}) and the solid black and red lines of *Atg7*$^{fl/fl}$ and *Atg7*$^{fl/fl}$ *Gzmb*-Cre origin (CD45.2^{+}), respectively. Each line represents data from one experimental mouse. Data are representative of two independent experiments.

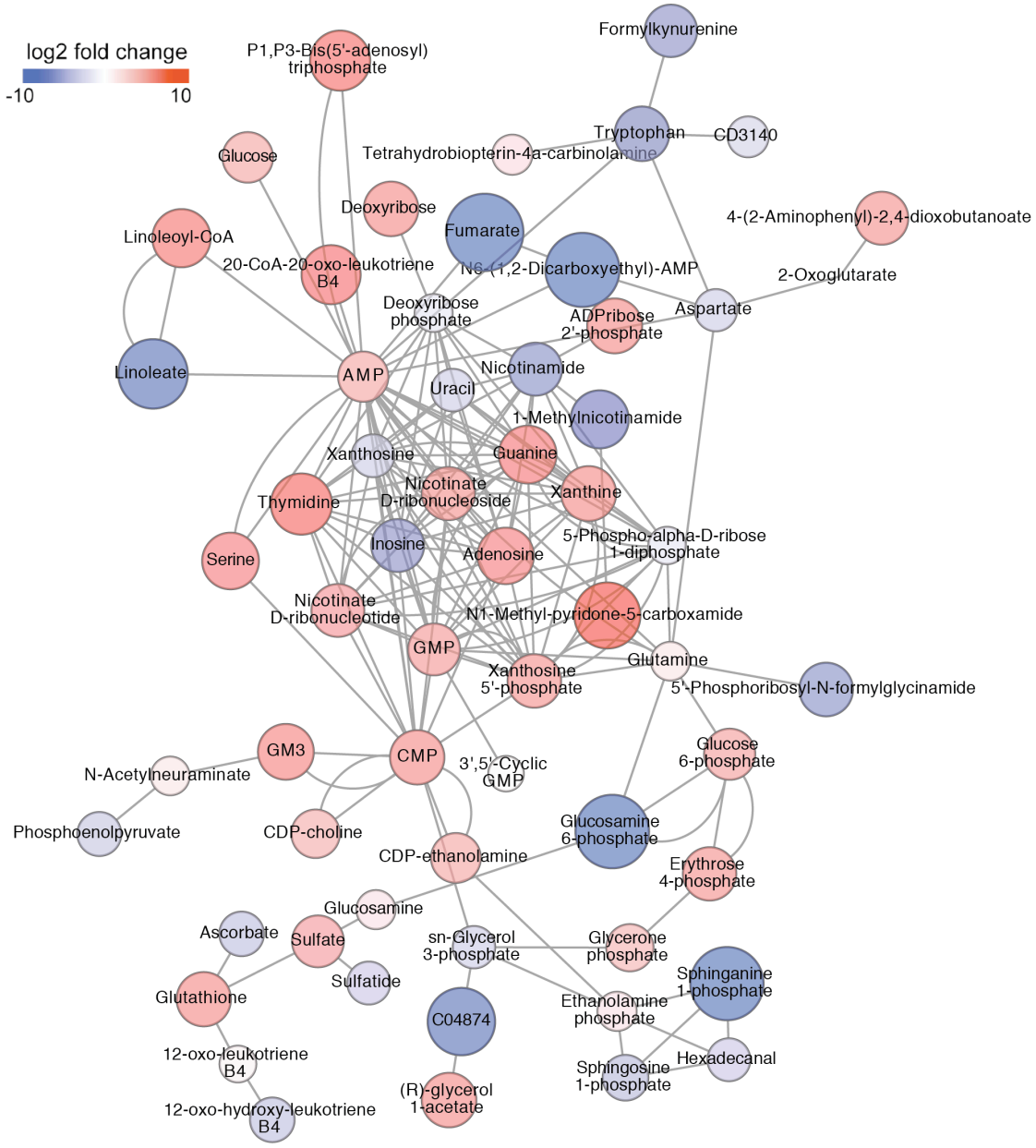

Supplementary Figure 6

Metabolic activity network of Atg7-deficient DbGP33 CD8 T cells.

Prediction directly from m/z feature tables (Supplementary Table 1) by method previously described[1]. Metabolites are colored according to log2 fold change.

1. Li, S. et al. Predicting network activity from high throughput metabolomics. PLoS Comput Biol 9, e1003123 (2013).

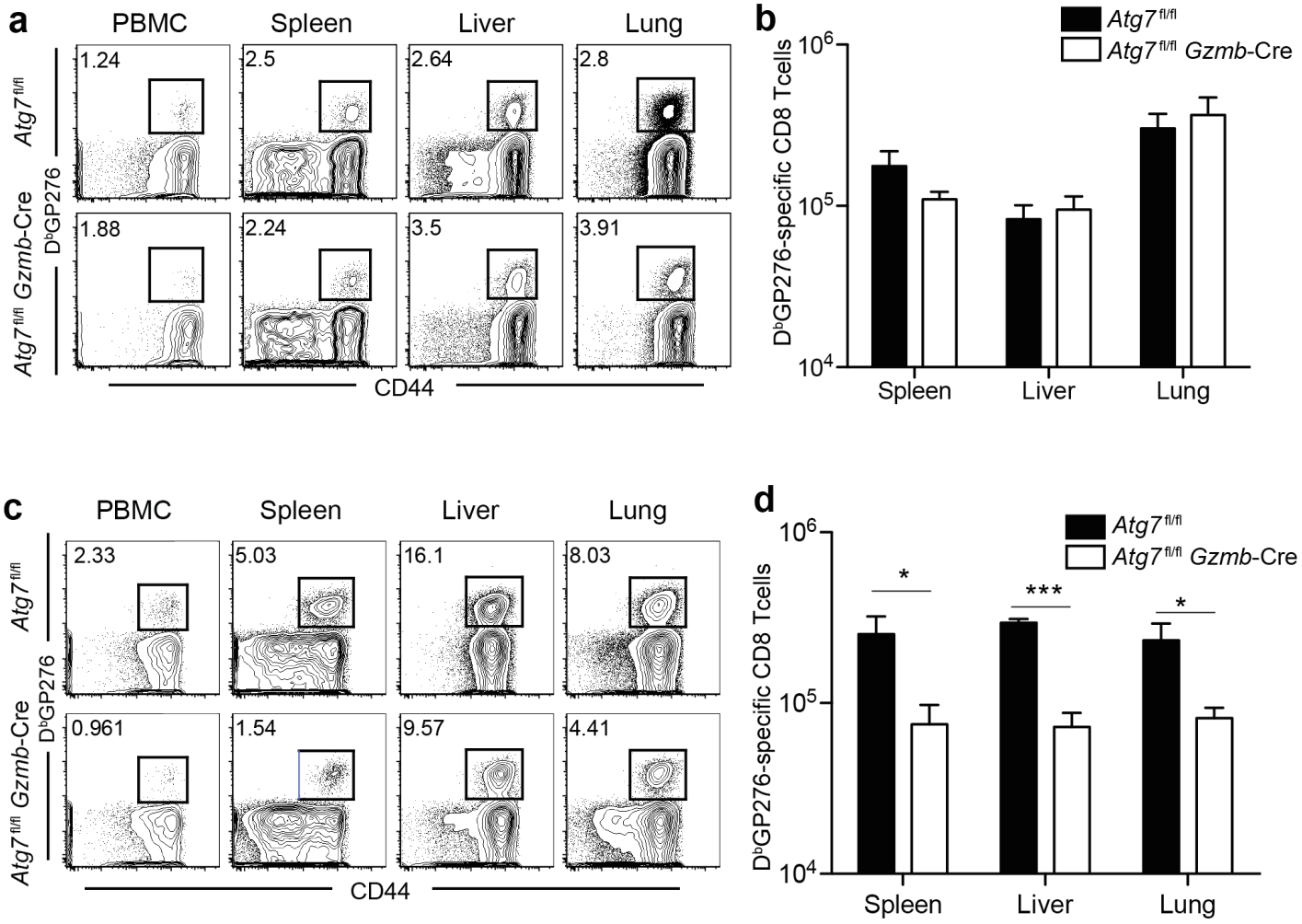

Supplementary Figure 7

Virus-specific CD8 T cell response during chronic LCMV infection in the absence of Atg7.

Atg7fl/fl Gzmb-Cre and control mice were infected with LCMV Clone-13. (**a**) and (**c**) Flow cytometric analysis of LCMV-specific T cells post LCMV Clone 13 infection in PBMC, spleen, liver and lung on days 8 and 15 p.i., respectively. The numbers on FACS plots indicate the percentage of D^bGP276-specific T cells on the gated CD8 T cells in each sample examined. (**b**) and (**d**) The total numbers of D^bGP276-specific T cells in each tissue are plotted at days 8 and 15 p.i., respectively. n=3-5 in each group. Data are representative of two independent experiments. Error bars indicate SEM. *, p≤0.05. ***, p≤0.0005